# Integrated Transcriptomic and Mendelian Randomization Analyses Identify Novel Biomarkers of Depression and Diabetes Comorbidity

**Yushan Xu**

xuyushan1019@126.com

The First Affiliated Hospital of Kunming Medical University

**Li Shi**
**Dandan Huang**
**Linkuai Zhu**
**Li Zhu**
**Na Li**
**Yang Liu**
**Yan Jiang**

**Article**

**Keywords:** Diabetes mellitus, Depressive disorder, comorbidity, Mendelian randomization, Actin-related protein 2/3 complex subunit 2, Autophagy-related protein 7

**Posted Date:** June 12th, 2026

**DOI:** https://doi.org/10.21203/rs.3.rs-9633629/v1



**Additional Declarations:** The authors have declared there is **NO** conflict of interest to disclose

# Integrated Transcriptomic and Mendelian Randomization Analyses Identify Novel Biomarkers of Depression and Diabetes Comorbidity

*Li Shi,PhD[a #]; Dandan Huang,MSc[a #]; Linkuai Zhu,MSc[a #]; Li Zhu,MSc[a]; Na Li,PhD[b]; Yang Liu,MSc[a]; Yan Jiang,MSc[a *]; Yushan Xu,PhD[a *]*

*[a] Endocrine and Metabolic Diseases Department，The First Affiliated Hospital of Kunming Medical University，Yunnan 650032,PR China*

*[b] Psychiatry，The First Affiliated Hospital of Kunming Medical University，Yunnan 650032,PR China*

**Corresponding authors at: Endocrine and Metabolic Diseases Department，The First Affiliated Hospital of Kunming Medical University，Yunnan 650032,PR China.*

*E-mail addresses: xuyushan1019@126.com(Yushan Xu); jyan_6@126.com (Yan Jiang).*

*# These authors have contributed equally to this work*

**Abstract**

Objective: Type 2 diabetes mellitus (DM) and depressive disorder (DD) frequently co-occur; however, the mechanisms underlying their comorbidity remain insufficiently understood. Therefore, the aim of this study was to explore the immune dysregulation mechanisms involved in the pathogenesis of DM and DD. Transcriptomic profiling was integrated with Mendelian randomization (MR) to investigate the potential causal roles of immune-related genes in DM and DD, and identify candidate targets associated with their comorbidity.

Method: MR analysis identified 21 candidate genes causally associated with DM and DD, including actin-related protein 2/3 complex subunit 2 (ARPC2) and autophagy-related protein 7 (ATG7), which were prioritized as key pathogenic genes. Functional enrichment and immune infiltration analyses further validated the MR results, confirming their association with immune-related pathways and immune cell infiltration. The expression of these genes was validated using *in vitro* and *in vivo* experiments.

Results: Increased ARPC2 and ATG7 expression was associated with an elevated risk of DM-DD. Gene set variation analysis (GSVA) and gene set enrichment analysis (GSEA) indicated significant enrichment of immune-related pathways associated with these genes.

Conclusion: ARPC2 and ATG7 were identified as candidate biomarkers of DM-DD comorbidity. These findings suggest that immune activation and autophagy-related pathways may contribute to the progression of DM-DD comorbidity.

**Keywords:** Diabetes mellitus; Depressive disorder; comorbidity; Mendelian randomization; Actin-related protein 2/3 complex subunit 2; Autophagy-related protein 7.

## 1. Introduction

Diabetes mellitus (DM) is one of the most prevalent metabolic disorders worldwide. China accounts for approximately one-quarter of the global DM population, ranking first in prevalence. This systemic chronic disease is characterized by multiple complications affecting vascular, neural, and various organs, and is closely associated with insulin resistance, immune dysfunction, and inflammatory responses (Yu et al., 2024; Lu et al., 2024). Accumulating evidence from recent clinical studies indicates that DM is significantly associated with cognitive impairment disorders (Wimberley et al., 2022). Associations between DM and depressive disorder (DD) have also been reported (Maina et al., 2023) (Habib et al., 2022). A bidirectional relationship between DD and DM has been described, with the prevalence of DD among diabetic patients being approximately twice that observed in non-diabetic individuals. Moreover, patients with both DM and DD exhibit poorer clinical outcomes and higher mortality rates compared to those affected by either condition alone (Gillett et al., 2024; Sarwar et al., 2022). This comorbidity is associated with a more severe disease course, poorer prognosis, greater functional impairment, and increased risks of complications, including suicide (Yadav et al., 2023). Conventional treatments targeting either DD or DM often fail to adequately address the shared pathophysiological mechanisms underlying both conditions (Li et al., 2024).

Therefore, further exploration of the co-pathogenic mechanisms linking these disorders and the identification of potential therapeutic targets are warranted.

The pathophysiological interactions between DD and DM are complex and multifactorial. Shared pathological mechanisms have been proposed and include inflammatory responses, oxidative stress, epigenetic alterations, and insulin resistance (Habib et al., 2022; Khawagi et al., 2024; Yao et al., 2025; Li et al., 2024). The potential interactions between DM and DD may occur through multiple immune-mediated pathways. Increasing empirical evidence supports a central role of immune dysregulation and chronic inflammation, with immune cell homeostasis imbalance and persistent immune activation identified as key contributing factors (Duarte-Silva et al., 2021). Immune activation exerts a direct stimulatory effect on the hypothalamic-pituitary-adrenal axis (Sudirman et al., 2024). Activated microglia aggravate intracranial inflammatory responses, thereby inducing neuronal damage and synaptic dysfunction. Inflammatory mediators disrupt neurotransmitter metabolic pathways and suppress neuroplasticity, ultimately contributing to depressive-like behavioral phenotypes. Concurrently, diabetes is characterized by chronic low-grade inflammation and impaired immune function, involving alterations in inflammatory mediators, autoimmune responses, and immune cell infiltration (Z. Zhou et al., 2024). Shared immunometabolic pathways may therefore facilitate the onset and progression of both disorders. Immune-related genes (IRGs) are involved in the pathogenesis of multiple diseases, including cancer, obesity, non-alcoholic fatty liver disease, and Alzheimer's disease (He et al., 2024; Ho-Plágaro et al., 2022; Song et al., 2023; Wilson et al., 2023). However, the specific role of IRGs in DM-DD comorbidity remains unclear. Although the contribution of immune mechanisms to disease comorbidity has been increasingly recognized, the specific molecular mechanisms and pathways involved remain insufficiently elucidated.

It was hypothesized that aberrant expression of specific genes may disrupt immune cell activation, leading to immune dysregulation and autophagy induction, thereby contributing to the onset and progression of DM-DD. To address this hypothesis, an integrative analytical framework combining transcriptomic profiling

with Mendelian randomization (MR) analysis was used and subsequently validated through *in vitro* and *in vivo* experimental approaches.

## 2. Materials and Methods

### 2.1. Data extraction

The datasets were obtained from the Gene Expression Omnibus (GEO, https://www.ncbi.nlm.nih.gov/geo/) database (DM training set: GSE95849; DM validation set: GSE15932; DD training set: GSE76826; DD validation set: GSE32280). IRGs were obtained from the ImmPort database (https://www.immport.org).

### 2.2. Identification of differentially expressed genes (DEGs)

Differential expression analysis was performed separately for the DD (disease *vs*. control) and DM datasets using the R package "limma". The thresholds were set as $|\log2FC| > 0$ *and* $P$ value $< 0.05$. Intersection analysis was performed using the "VennDiagram" package (version 1.7.3) to identify genes consistently dysregulated in both DM and DD, as well as those overlapping with IRGs. Gene Ontology (GO) and Kyoto Encyclopedia of Genes and Genomes (KEGG) enrichment analysis were carried out on the screened DEGs using the "clusterProfiler" package in R to identify their shared biological functions and associated pathways. Additionally, a protein-protein interaction (PPI) network was constructed using Cytoscape (version 3.9.1).

### 2.3. Screening of key genes using MR Analysis

MR analysis was performed to assess the causal relationships between candidate genes and the risk of DD and DM with each candidate gene treated as the exposure and DD or DM as the outcome (D. Zhou et al., 2024). Genes showing a statistically significant causal effect based on the inverse variance weighted (IVW) method ($P < 0.05$) were defined as key causal genes.

### 2.4. Screening of biomarkers based on expression analysis

The Wilcoxon rank-sum test was used to compare the expression of key genes identified in Section 2.3 between DM and DD blood samples and corresponding control blood samples. Genes showing consistent and statistically significant

differential expression ($P < 0.05$) in the same direction across both their respective training and validation datasets were selected as final candidate biomarkers.

### 2.5. Nomogram construction and evaluation

A nomogram was constructed using the R package "rms" (regression modeling strategies). The predictive performance and clinical utility of the nomogram were evaluated by decision curve analysis (DCA) using the R package "ggDCA". DCA was performed to quantify the net clinical benefit of the prediction model across different threshold probabilities.

### 2.6. Gene set enrichment analysis (GSEA)

Spearman correlation coefficients were calculated between each biomarker and all other genes in the DM and DD training datasets using the `cor` function in R to further investigate the biological functions and signaling pathways associated with the biomarkers in DM and DD. The resulting correlation coefficients for each biomarker were used as the ranking metric for subsequent analysis. GSEA was performed using the "clusterProfiler" package against the c2.cp.kegg.v2023.1.Hs.symbols.gmt gene set (curated canonical pathways) obtained from the Molecular Signatures Database. Significant enriched pathways were identified based on $|NES| > 1$, $FDR < 0.25$, and $P < 0.05$.

### 2.7. Gene set variation analysis (GSVA)

Gene sets from the Molecular Signatures Database were used as the reference to assess pathway-level differences between the disease and control groups. The R package "GSVA" was used to perform GSVA to calculate enrichment scores for all samples in the DM and DD training sets. Differential analysis of GSVA scores between disease and control groups was subsequently performed using the "limma" package in R. Significantly enriched gene sets were visualized using a heatmap generated with the "pheatmap" function. Additionally, a lollipop chart (or comparable visualization such as a dot plot) was created using "ggplot2" to clearly display enrichment levels of these gene sets (c2.cp.kegg.v2023.1.Hs.symbols.gmt).

### 2.8. Immune infiltration analysis

Immune cell infiltration levels were compared between DM and control groups (disease *vs*. control) across 28 immune cell types using Wilcoxon rank-sum test, with a statistically significant threshold of $P < 0.05$. A total of 13 immune-infiltrating cells with significantly different infiltration levels were identified and designated as DM-associated immune cells. Similarly, 12 immune cell types were identified as DD-associated immune cells using the same analytical approach. Spearman correlation analysis was subsequently performed between differentially infiltrating immune cells and identified biomarkers in the DM training set GSE95849 using the "corrplot" package (version 0.92). This analysis compared DM blood samples with control blood samples (disease *vs* control). The analysis was based on an absolute correlation coefficient threshold of $|cor| > 0.3$ and $P < 0.05$. The minimum absolute correlation coefficient was set at 0.3, although this threshold remained adjustable.

### 2.9. GeneMANIA analysis and subcellular localization

GeneMANIA analysis was performed to investigate the functional interaction of the identified biomarkers in DD and DM. The FASTA sequences of ARPC2 and ATG7 were obtained from public databases, and their subcellular localization was predicted using the mRNALocater database (http://bio-bigdata.cn/ mRNALocater/).

### 2.10. Molecular regulation network construction

The miRDB database (https://mirdb.org/) was used to predict the potential candidate miRNA targeting the identified genes to explore potential regulatory mechanisms and identify putative binding sites of biomarkers, The Knock TF database (https://bio.liclab.net/ KnockTF/index.p) was used to investigate interactions between key genes and transcription factors (TFs). Cytoscape software was subsequently used to visualize mRNA-miRNA interactions and construct TF-mRNA regulatory networks.

### 2.11. Animal experiments

This study was approved by the Animal Research Ethics Committee of Kunming Medical University (Ethics Code: kmmu2021426) and was performed according to institutional guidelines for animal care and use. Five-week-old male Kunming mice, each weighing 18-22 g (n = 15 per group; total n = 60) were purchased from Hunan

Sile Jinda Experimental Animal Co. Ltd. (License: SCXK (Xiang) 2019-0004). Mice were randomly divided into four groups: control (CON), DD, DM and combined DM-DD. DM was induced by feeding mice a high-fat diet for 6 weeks. After a 16-hour fasting, streptozotocin (STZ) was administered through an intraperitoneal injection at a dose of 200 mg/kg body weight over three days: 100 mg/kg on day 1, 50 mg/kg on day 2, and 50 mg/kg on day 3. Control mice were subjected to the identical protocol but received citrate buffer. Mice with fasting blood glucose levels ≥ 200 mg/dl were considered diabetic. A depression model was established using a chronic mild unpredictable stress-induced protocol, consisting of the daily application of one randomly selected stressor. Ten stressors were randomly applied in a randomized manner 2-3 times cumulatively: fasting, water deprivation, cold water (4 °C) swimming, tail pinching, environmental heat exposure (45 °C), intermittent noise exposure, 24-hour circadian rhythm reversal, footpad electric shock, shaking, and exposure to unfamiliar odors. The stress protocol was maintained for 28 consecutive days. Behavioral assessment revealed significantly reduced escape latency, total movement distance, and speed in the depression group compared with the control group. The DM-DD comorbidity model was established by combining the protocols used to induce both diseases. After model establishment, body weight was recorded and biological samples were collected. Pancreatic and hippocampal tissues were rapidly harvested, snap-frozen in liquid nitrogen and stored at -80 °C. PCR and Western blot (WB) analyses were subsequently performed on hippocampal and pancreatic tissues.

### 2.12. Cell culture

The mouse hippocampal neuronal cell line HT22 was cultured under standard conditions (37 °C, 5% $CO_2$) in DMEM powder medium supplemented with penicillin-streptomycin solution, fetal bovine serum (FBS), and 25 mM glucose. The normal control group (Ctrl) was cultured under identical basal conditions and corresponded to Group I. Three groups were established by adjusting glucose and cortisol concentrations in the culture medium: Group II (HT22 + 75 mM glucose, HG), Group III (HT22 + 100 μM cortisol, CORT), and Group IV (HT22 + 75 mM

glucose + 100 μM cortisol, HG+CORT). Cells were seeded into a 96-well plate, exposed to the indicated treatments for 6, 12, 24, 48, and 72 hours, and viability was assessed using CCK-8 assay. Briefly, the culture supernatant was removed, and 100 μl basal medium was added to each well, including the blank control well. Next, 10 μl CCK-8 solution was added to each well, and plates were incubated in the dark for 2 hours. Finally, the absorbance was measured at 450 nm using an ELISA microplate reader (Osheng Feyond-A300). Following viability assessment, cells were collected for subsequent analyses.

### 2.13. Behavioral experiment

Open field testing and Morris water maze were performed to evaluate the cognitive function, emotional behavior, and spontaneous locomotor ability in mice. Open field test: each mouse was placed in the center of an open-field box and allowed to explore freely for 5-10 min. Movement trajectories were recorded using an automated video system. The analyzed parameters included total distance traveled, time spent in the central area, and the ratio of central area duration to total distance traveled, with all data processed through an automated software analysis. Morris water maze test: mice were placed in a circular pool filled with water and trained to locate a submerged platform hidden beneath the water surface. Training was conducted for 4 consecutive days and the platform was removed on the 5th day to perform a probe trial assessing spatial memory retention. Escape latency during training, time spent in the target quadrant during testing, and the number of crossings over the former platform location were recorded. All data were analyzed using automated software.

### 2.14. Quantitative polymerase chain reaction (q-PCR)

Total RNA was extracted from mouse hippocampal tissue, mouse pancreatic tissue, and HT22 cells using TRIzol reagent (Thermo Fisher Scientific Cat. No. 15596-018) according to the manufacturer's instructions. cDNA was synthesized from mRNA using the FastKing RT Kit with gDNase (Tiangen, Cat. No. KR116-02), and the resulting first-strand cDNA was used as the template for q-PCR amplification. The mRNA sequences of the target genes of the corresponding species were found on PubMed and primers were designed accordingly using Beacon Designer 7.90 with the

following sequences (see the attached table for the specific sequence). qPCR reactions were performed using a Roche LightCycler 96 system (Roche Diagnostics).

2.15. WB

Mouse tissues or HT22 cells were lysed in RIPA lysis buffer and homogenized using a homogenizer (60 Hz for 60 s). Total protein was quantified using an IMPLEN Nanophotometer Ultra-trace spectrophotometer (model T51017). Equal amounts of protein (80 μg) were separated by SDS-PAGE electrophoresis on 10% or 15% gels and subsequently transferred onto a PVDF membrane using a wet transfer system. The membrane was blocked with 5% skim milk or bovine serum albumin (BSA) at room temperature for 2 hours. The membrane was washed with TBST buffer and incubated overnight at 4 °C with primary antibodies under shaking. Following additional TBST washing, the membrane was incubated with secondary antibodies at room temperature for 2 hours. Protein bands were visualized using an enhanced chemiluminescence (ECL) detection system and imaged using a Tanon Light Emitting Imager (model 5200 Multi).

2.16. Enzyme-linked immunoassay (ELISA)

The expression of the neurotransmitters 5-HT, DA, and NE was measured in the cell groups mentioned in the paragraph 2.12 using commercial ELISA kits (EnzymeLink Biotech) according to the manufacturer's instructions. The sample was added to a microplate pre-coated with a captured antibody. After binding of the target protein, detection antibodies and enzyme-conjugated reagents were added to form a sandwich complex. Substrate solution was added and the absorbance was measured at 450 nm to quantify the concentration of target proteins. The equipment used included an electric thermostatic drying oven (Shanghai Senxin DGG-9140B), high-speed refrigerated centrifuge (Thermo Scientific), micropipettes (Eppendorf), refrigerator (Haier 4 ℃/-20 ℃), and ELISA plate reader (ALLSHENG Feyond-A300).

2.17. Immunofluorescence staining

Cells were fixed with 4% paraformaldehyde at 4 ℃ for more than 30 min and subsequently washed with PBS. Permeabilization was performed using 0.1% Triton X-100 for 15 min, followed by additional PBS washes. Non-specific binding was

blocked with 5% BSA at 37 ℃ for 60 min. Cells were then incubated with primary antibodies overnight at 4 ℃. After washing, appropriate fluorescent secondary antibodies were applied and incubated at 37 ℃ for 60 min. Nuclei were counterstained using DAPI-containing mounting medium and slides were sealed for imaging.

2.18. Statistical analysis

Statistical analysis was performed using GraphPad Prism 10.1.2. software. One-way ANOVA was used for comparisons among multiple groups. The Brown-Forsythe test was used to assess variance homogeneity, followed by Sidak's multiple comparison test. Results were presented as mean ± standard deviation (SD). A value of $P < 0.05$ was considered statistically significant.

## 3. Results

3.1 Identification of 322 candidate genes associated with DM, DD and IRGs

Differential gene expression analysis was performed between the disease and control groups in the training dataset to explore shared molecular alterations. A total of 5,593 differentially expressed genes were found between the DD disease group and the normal group, with 3,551 upregulated genes and 2,042 downregulated genes (Figure 1A-B). A total of 6,307 differentially expressed genes were found between the DM group and the normal control group, with 5,291 upregulated genes and 1,016 downregulated genes (Figure 1C-D). Overlapping analysis to reveal genes exhibiting consistent expression trend in both DM and DD revealed 1,405 co-disease DEGs comprising 1,368 upregulated genes and 37 downregulated genes (Figure 1E-F). Further intersection of these co-disease DEGs with IRGs yielded 322 candidate genes (Figure 1G).

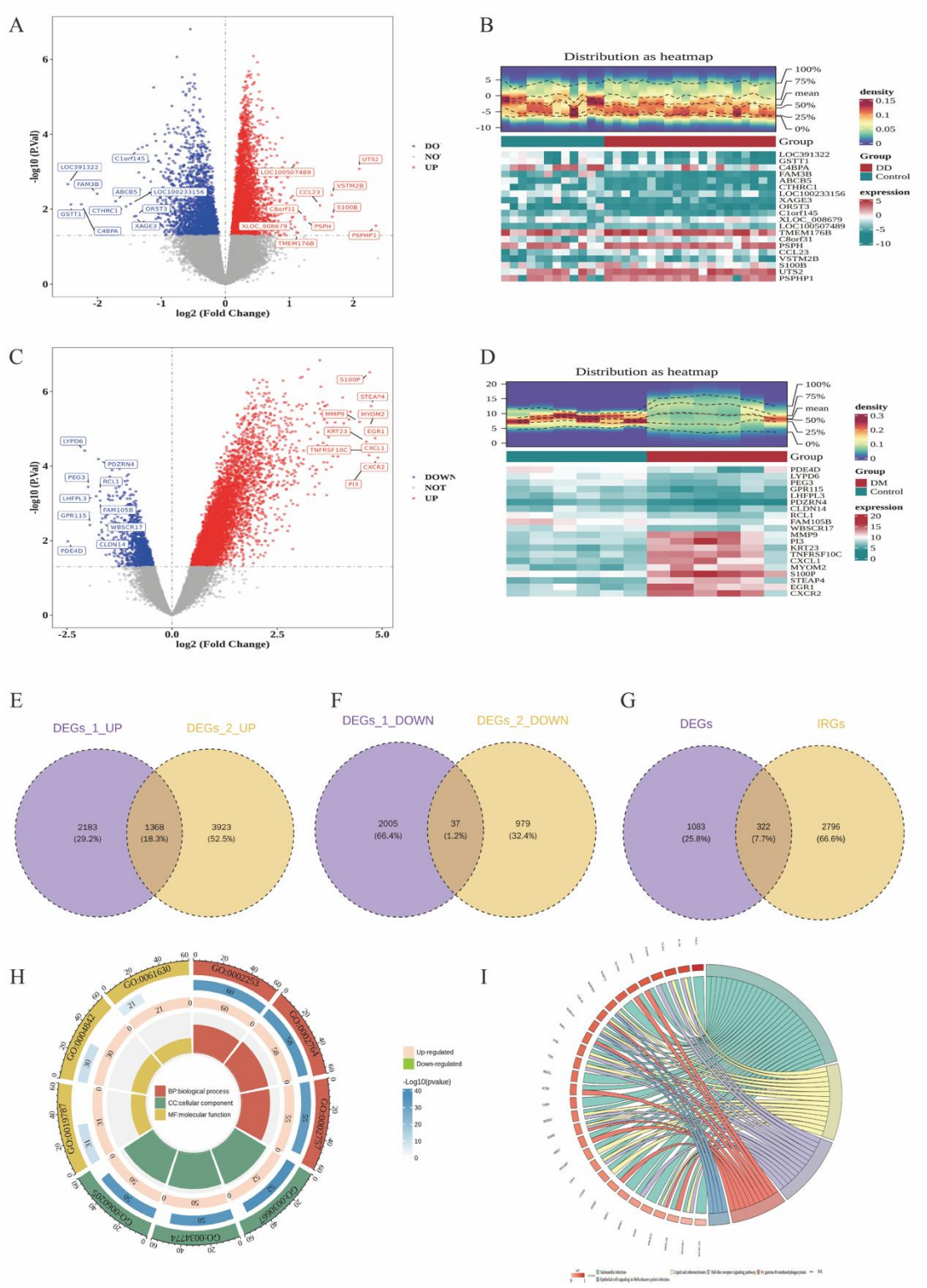


**Figure 1. Identification of DEGs-1, DEGs-2, DEGs, candidate genes, KEGG and GO enrichment analysis.**

**(A-B)** DEGs-1 volcano plot and heatmap.

**(C-D)** DEGs-2 volcano plot and heatmap.

**(E-F)** Venn diagrams showing the intersection of genes upregulated and

downregulated in DM and DD, respectively.

**(G)** Venn diagram of candidate genes obtained through the intersection of comorbidity DEGs and IRGs.

**(H)** GO enrichment analysis of candidate genes.

**(I)** KEGG pathway enrichment analysis of candidate genes.

3.2 Functional enrichment analysis of candidate genes using GO and KEGG.

GO and KEGG enrichment analyses were performed to elucidate the biological functions and pathways associated with the 322 candidate genes. GO enrichment analysis identified a total of 1620 significant terms, including 1329 biological processes (BP), 151 cellular components (CC), and 40 molecular functions (MF). Within the BP category, candidate genes were significantly enriched in immune-related processes, including activation of immune responses (GO:0002253), immune response modulation signaling pathway (GO:0002764), immune response activating signaling pathway (GO:0002757), positive regulation of defense responses (GO:0031349), and regulation of biostimulus response (GO:0002831). In the CC category, significant enrichment was observed in secretory granular membranes (GO:0030667), secretory granular cavity (GO:0034774), cytoplasmic vesicle cavity (GO:0060205), vesicular lumen (GO:0031983), and ficolin-1-rich particles (GO:0101002). In the MF category, enrichment was detected in ubiquitin-like protein transferase activity (GO:0019787), ubiquitin-protein transferase activity (GO:0004842), ubiquitin protein ligase activity (GO:0061630), ubiquitin-like protein ligase activity (GO:0061659), and actin binding (GO:0003779) (Figure 1H).

KEGG pathway enrichment analysis identified 46 significantly enriched pathways, and candidate genes were associated with Salmonella infection (hsa05132), lipid and atherosclerosis (hsa05417), Toll-like receptor signaling pathway (hsa04620), FcγR-mediated phagocytosis (hsa04666), and epithelial cell signaling in Helicobacter pylori infection (hsa05120) (Figure 1I).

3.3 Causal relationship of candidate genes with DD and DM identified through MR

MR analysis was performed to investigate potential causal associations between the 322 candidate genes and the risk of DM and DD. A total of 75 genes were identified

as associated with DM, while 68 genes were associated with DD. The intersection of these two gene sets yielded 21 shared key genes. Among the identified genes, ATG7 exhibited a significant negative causal association with DM (Figure 2A), indicating a potential protective effect against DM risk. Similarly, inverse variance weighted analysis demonstrated a negative causal association between ATG7 and DD (Figure 2B). Assessment of instrumental variable validity indicated no apparent violation of MR assumptions. The distribution of instrumental variables was approximately symmetrical in the funnel plot (Figure 2C), suggesting minimal bias. Sensitivity analyses, including heterogeneity testing, horizontal pleiotropy assessment, and leave-one-out analysis (Figure 2D) further supported the robustness and reliability of the causal estimates. A total of 21 shared key genes were identified through the intersection of DM- and DD-associated genes, highlighting potential common causal mediators (Figure 2E).

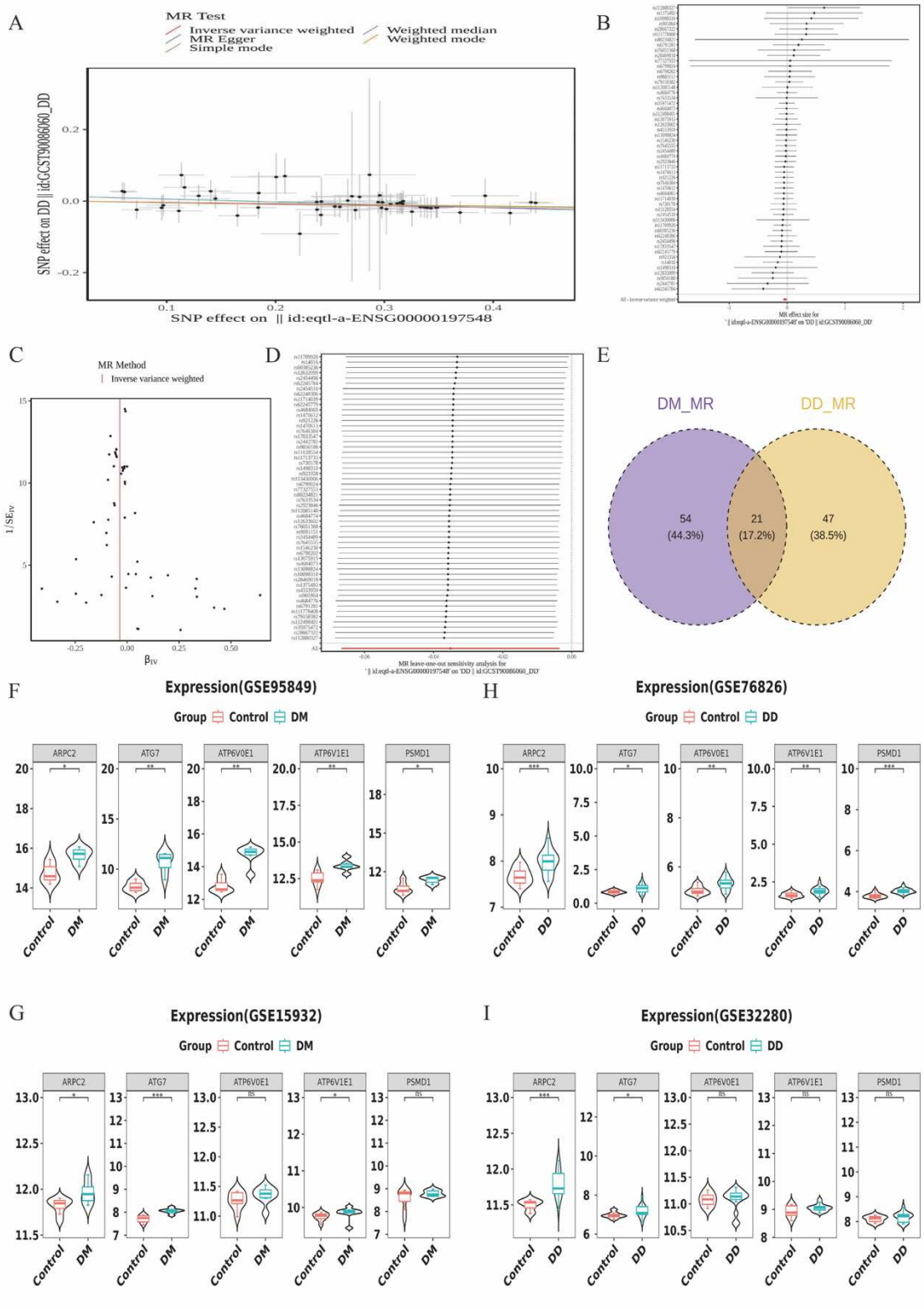


**Figure 2. MR identified key genes associated with DD and DM**

**(A)** Scatter plot showing the association between ATG7 expression and DD risk.

**(B)** Causal effect estimates of ATG7 on DD based on IVW.

**(C)** Randomness assessment of candidate exposure factors.

**(D)** Leave-one-out sensitivity analysis evaluating the stability of causal estimates.

**(E)** Venn diagram illustrating the overlap between DM-associated and DD-associated genes identified by MR analysis. A total of 21 shared key genes were obtained from the intersection.

**(F-G) Expression-based biomarker screening in** DM training and validation datasets.

**(H-I) Expression-based biomarker screening in** DD training and validation datasets.

3.4 Identification of key genes with consistent expression in DD and DM training and validation datasets

The expression profiles of key genes were evaluated to identify biomarkers exhibiting stable expression patterns across datasets in both training and validation cohorts of DM and DD. ARPC2, ATG7, and ATP6V1E1 were significantly differentially expressed in the DM datasets (Figure 2F-G). ARPC2 and ATG7 demonstrated consistent differential expression in the DD datasets (Figure 2H-I). Among them, ARPC2 and ATG7 showed significantly upregulated expression in both DD and DM and were therefore selected as shared biomarkers through intersection analysis.

3.5 Evaluation of the predictive value of ARPC2 and ATG7 for DM and DD

Predictive nomograms were constructed for DM and DD to evaluate the diagnostic performance of ARPC2 and ATG7. The total score derived from gene expression levels was used to estimate disease probability, with higher scores corresponding to increased prevalence (Figure 3A-B). The results showed that the prevalence of DD was higher than that of DM.

Decision curve analysis demonstrated that the predictive models provided a greater net benefit than both the “treat-all” and “treat-none” strategies across a range of threshold probabilities (Figure 3C-D), indicating favorable clinical utility.

Calibration analysis further revealed good agreement between predicted and observed probabilities. The calibration curves showed slopes close to 1, with a $P$ value > 0.05, indicating that the predictive performance of the model was relatively accurate (Figure 3E-F).

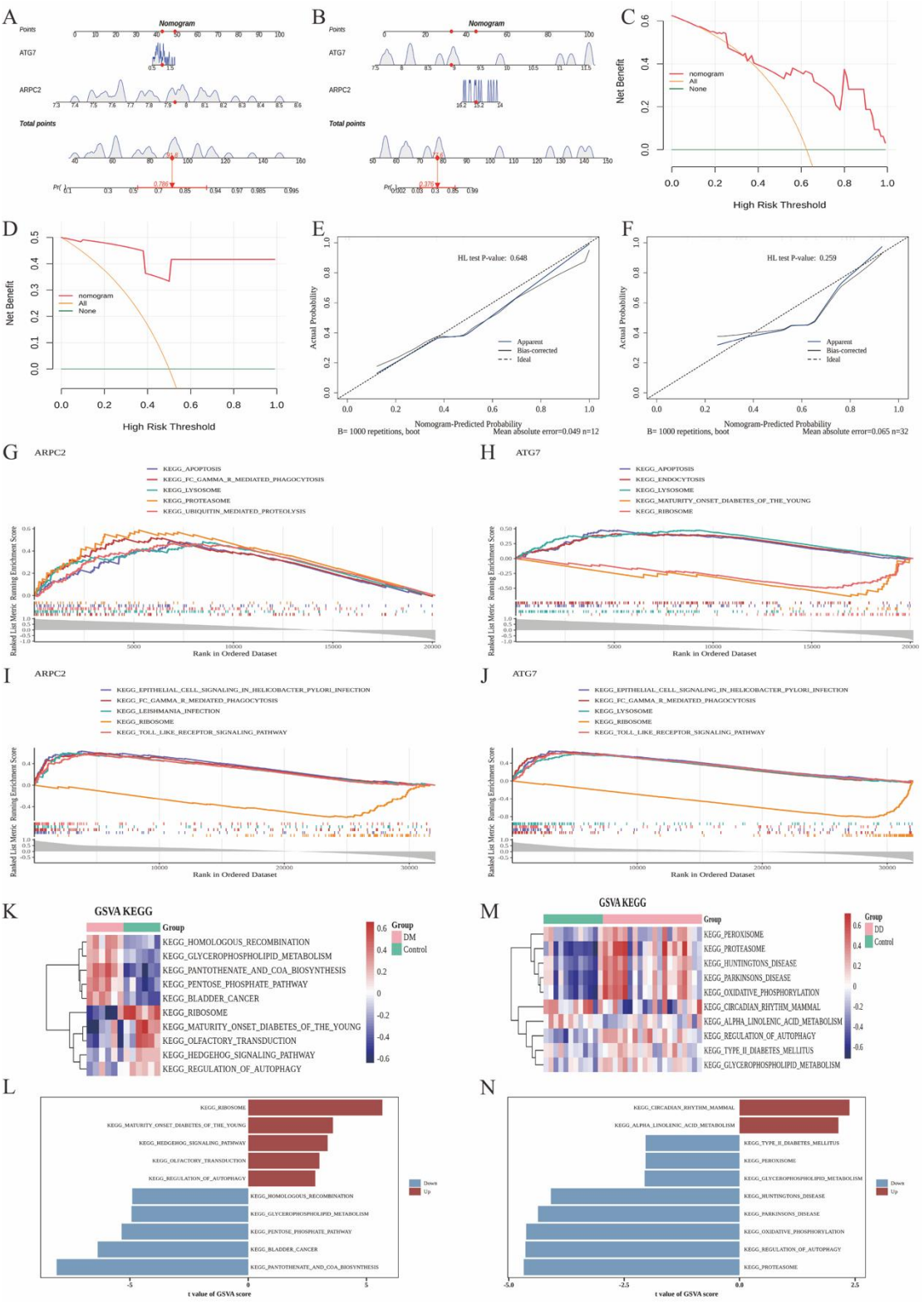


**Figure 3. Predictive performance of ARPC2 and ATG7 and functional enrichment analysis.**

**(A)** Nomogram for predicting DD risk based on ARPC2 and ATG7 expression.

**(B)** Nomogram for predicting DM risk based on ARPC2 and ATG7 expression.

**(C)** DCA curve for the DD prediction model.

**(D)** DCA curve for the DM prediction model.

**(E)** Calibration curve of DM prediction model.

**(F)** Calibration curve of the DD prediction model.

**(G-H)** GSEA-KEGG enrichment analysis of ARPC2 and ATG7 in DM samples.

**(I-J)** GSEA-KEGG enrichment analysis of ARPC2 and ATG7 in DD samples.

**(K-L)** GSVA-KEGG analyses in DM samples.

**(M-N)** GSVA-KEGG analyses in DD samples.

3.6 Biomarker enrichment analysis

GSEA analysis in DM samples showed that ARPC2 and ATG7 were mainly enriched in apoptosis, lysosomal composition, ubiquitin-mediated proteolysis, FcγR-mediated phagocytosis, ribosomal function, endocytosis, and maturity-onset diabetes of the young. GSEA analysis in DD samples showed enrichment mainly in epithelial cell signaling, FcγR-mediated phagocytosis pathway, Leishmania infection, ribosome composition, Toll-like receptor signaling, lysosomal composition, and ribosomal composition in Helicobacter pylori infection (Figure 3G-J).

GSVA analysis showed significant pathway-level differences between disease samples and control samples. In DM, significant alterations were observed in ribosomal composition, maturity-onset diabetes of the young, Hedgehog signaling pathway, homologous recombination process, glycerol phospholipid metabolism and related physiological functions, pantothenic acid and coenzyme A biosynthesis. In DD, significant differences were identified in circadian mammal-related biological processes, α-linolenic acid metabolism, proteasome composition, autophagy signaling pathway, and oxidative phosphorylation processes (Figure 3K-N).

3.7 Immune infiltration characteristics and functional annotation of ARPC2 and ATG7

Immune infiltration analysis revealed 13 significantly altered immune cell types in DM, including antibody-secreting B cells, central memory CD4, and monocytes. In addition, 12 differentially abundant immune cell types were detected in DD, including antibody-secreting B cells, macrophages, and neutrophils. Positive correlations were predominantly observed among differentially infiltrating immune cells, and a

significant positive correlation was found between immune cell abundance and biomarker expression (Figure 4A-F). GeneMANIA database indicated that ARPC2 and ATG7 were functionally associated with 20 genes (Figure 4H). Subcellular localization analysis showed that both ATG7 and ARPC2 were mainly localized in the nucleus and cytoplasm (Figure 4G). TF-mRNA-miRNA network analysis showed that ATG7 and ARPC2 were modulated by multiple TFs and miRNAs (Figure 4I-J). Drug prediction and molecular docking analyses identified 1,013 candidate compounds targeting ATG7, with the top five being peptichemio, teniposide, ferumoxides, pravastatin, and interleukin-4 (Figure 4L). A total of 58 potential drugs were predicted for ARPC2, with the top five being hydrogen peroxide, sargramostim, cholesterol, interferon-gamma, and omega-3 fatty acid (Figure 4K).

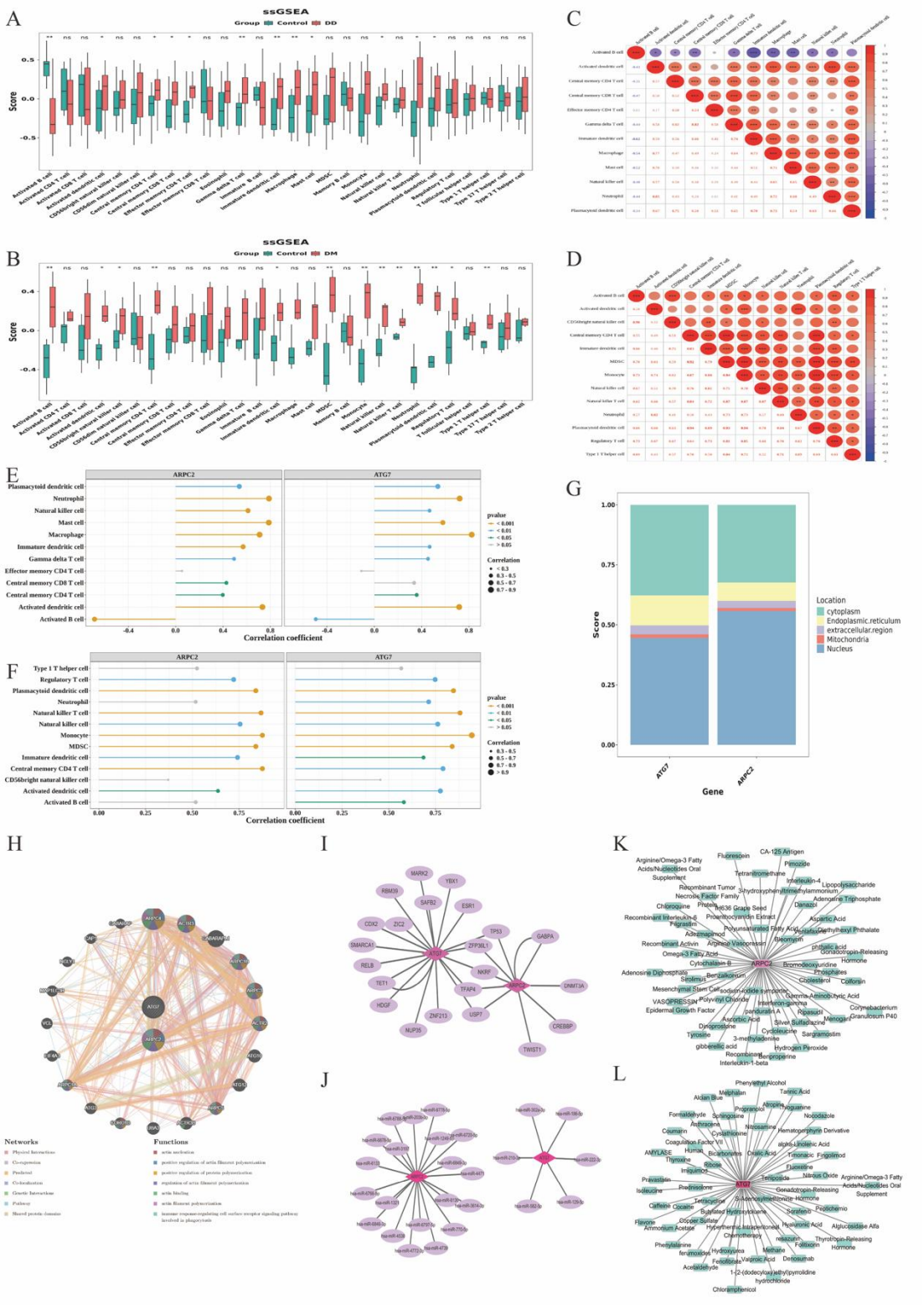


**Figure 4. Functional and regulatory characterization of ARPC2 and ATG7.**

**(A)** Differential immune cell infiltration between DD and control samples.

**(B)** Differential immune cell infiltration between DM and control samples.

**(C-D)** Correlation analysis among differentially infiltrating immune cells.

**(E-F)** Correlation between ARPC2 and ATG7 expression and differential immune cell abundance shown as lollipop plots.

**(G)** Subcellular localization of ARPC2 and ATG7.

**(H)** GeneMANIA interaction network of ARPC2 and ATG7.

**(I)** TF-mRNA regulatory network.

**(J)** miRNA-mRNA regulatory network.

**(K)** Predicted drug-gene interaction network for ARPC2.

**(L)** Predicted drug-gene interaction network for ATG7.

3.8 Behavioral alterations and upregulation of ARPC2 and ATG expression in the hippocampus and pancreas of DM-DD mice

Spontaneous activity and anxiety-like behavior were assessed in mice using the open-field test to evaluate the behavioral effects of DM, DD, and their comorbidity. Mice in the DM and DD groups showed reduced average speed, decreased total distance traveled and lower rearing frequency, accompanied by prolonged immobility time compared with the CON group ($P < 0.01$) (Figure 5B-E). The DM-DD group showed more pronounced anxiety- and depression-like behaviors. Average speed, total distance and rearing frequency were reduced compared with the DM and DD groups, while immobility time was significantly prolonged compared with the DD group ($P < 0.01$).

Spatial learning and memory revealed that mice in the DM and DD groups had a reduced average speed and total swimming distance, together with prolonged escape latency and immobility time compared with the CON group (Figure 5F-I). The DM-DD group exhibited longer escape latency than the DM and DD groups. Additionally, average speed and total distance were decreased in the DM-DD group compared with the DM and DD groups. Immobility time was significantly prolonged in the DM-DD group compared with the DD group ($P < 0.001$).

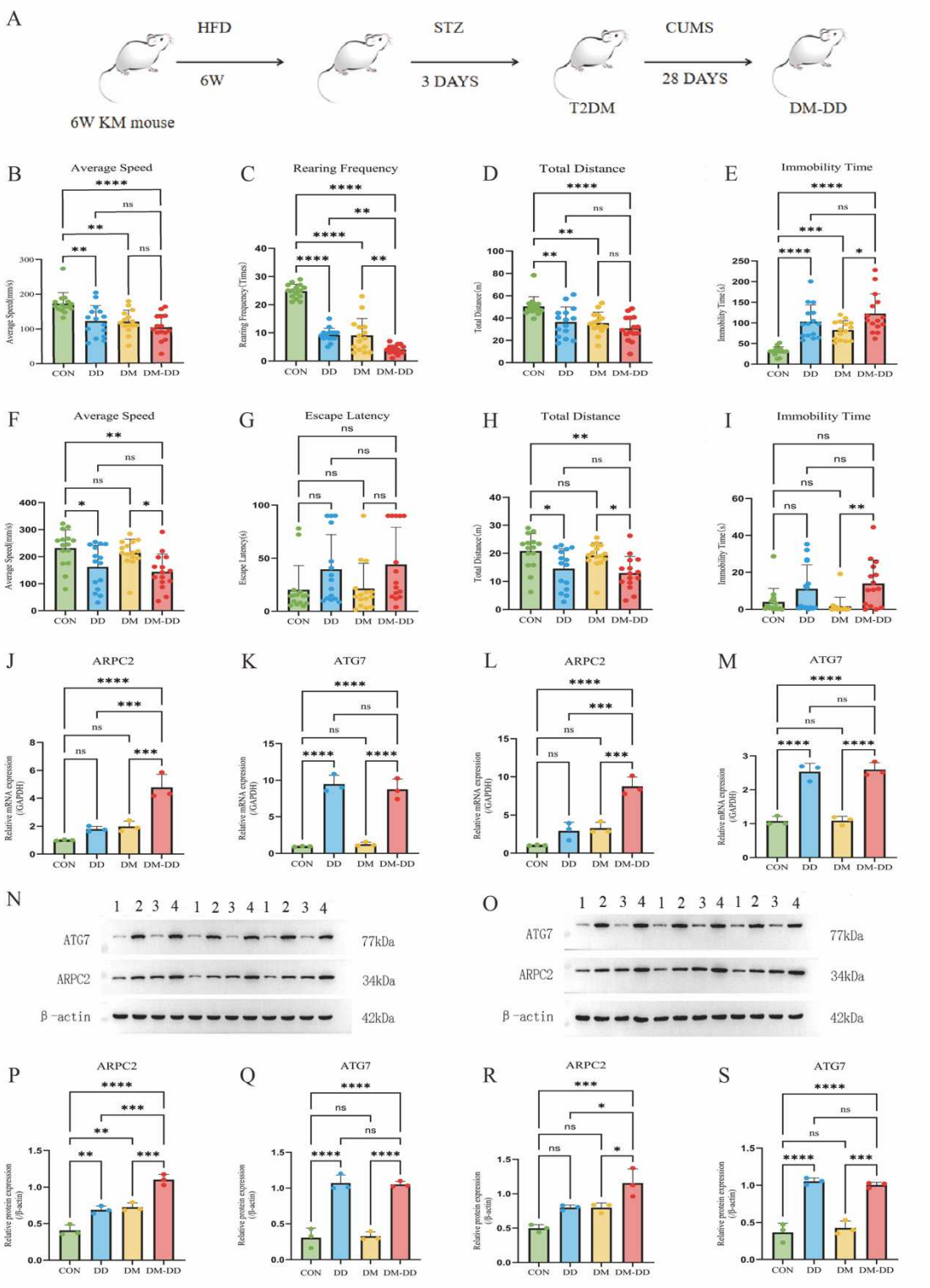


**Figure 5. Behavioral validation of the DM-DD model and expression analysis of ARPC2 and ATG7.**

**(A)** Schematic diagram of DM-DD animal modeling (high-fat diet [HFD], streptozotocin [STZ], and chronic unpredictable mild stress [CUMS]).

**(B-E)** Open field test results, including average speed (B), rearing frequency (C), total distance traveled (D), and immobility time (E).

**(F-I)** Morris water maze results, including average speed (F), escape latency (G), total distance traveled (H), and immobility time (I).

**(J-K)** qPCR of ARPC2 and ATG7 mRNA expression in mouse hippocampus

**(L-M) q**PCR of ARPC2 and ATG7 mRNA expression in mouse pancreas.

**(N-O) Representative WB images of ARPC2 and ATG7 expression in hippocampus (N) and pancreas (O). Groups are labeled as** 1 = CON, 2 = DD, 3 = DM, and 4 = DM-DD.

**(P-Q)** Quantification of ARPC2 and ATG7 protein expression in mouse hippocampus.

**(R-S)** Quantification of ARPC2 and ATG7 protein expression in mouse pancreas (ns = not significant, *$P < 0.05$, **$P < 0.01$, ***$P < 0.001$, ****$P < 0.0001$).

ATG7 and ARPC2 expression was evaluated in mouse hippocampal and pancreatic tissues to investigate the molecular basis underlying these behavioral alterations (Figure 5J–S). ARPC2 protein expression in the hippocampal tissues of the DM and DD groups was upregulated compared with that in the CON group ($P < 0.01$). ATG7 gene and protein expression were significantly upregulated in the DM-DD group compared with those in the DM group, and similar expression patterns were observed in the pancreatic tissue ($P < 0.001$). ARPC2 expression was increased in the DM-DD group than in both the DM and DD groups ($P < 0.001$). ARPC2 expression in the pancreatic tissue (Figure 5L-M, O, R-S) of the DM and DD groups was higher than that in the CON group ($P < 0.05$). ATG7 expression was significantly increased in the DD group compared with the CON group ($P < 0.0001$). The expression of these two genes was higher in the DM-DD group than in the DM group ($P < 0.001$).

3.9 Upregulation of ARPC2 and ATG7 expression in the HG + CORT cell model and neuronal localization

A high-glucose (HG), cortisol (CORT), and combined HG + CORT cell model was constructed to further investigate the cellular mechanisms underlying DM-DD

comorbidity. The experimental design of the cellular model is shown in Figure 6A. Cell viability was significantly reduced in both the HG and CORT groups compared with the Ctrl group, and was further decreased in the HG + CORT group (Figure 6B). Apoptotic rates were significantly increased in the HG and CORT groups compared with the Ctrl group, and were further increased in the HG + CORT group compared with both single-treatment groups (Figure 6C) ($P < 0.0001$). Glucose consumption was significantly increased in the HG and CORT groups compared with the Ctrl group (Figure 6D) ($P < 0.0001$). Glucose consumption was further enhanced in the HG + CORT group compared with the HG and CORT groups ($P < 0.0001$). Analysis of neurotransmitter levels in cell culture supernatants showed a significant reduction in 5-hydroxytryptamine (5-HT), dopamine (DA), and norepinephrine (NE) levels in the HG, CORT, and HG + CORT groups compared with the Ctrl group. Furthermore, neurotransmitter levels were further decreased in the HG + CORT group compared with the HG and CORT groups (Figure 6E-G) ($P < 0.05$).

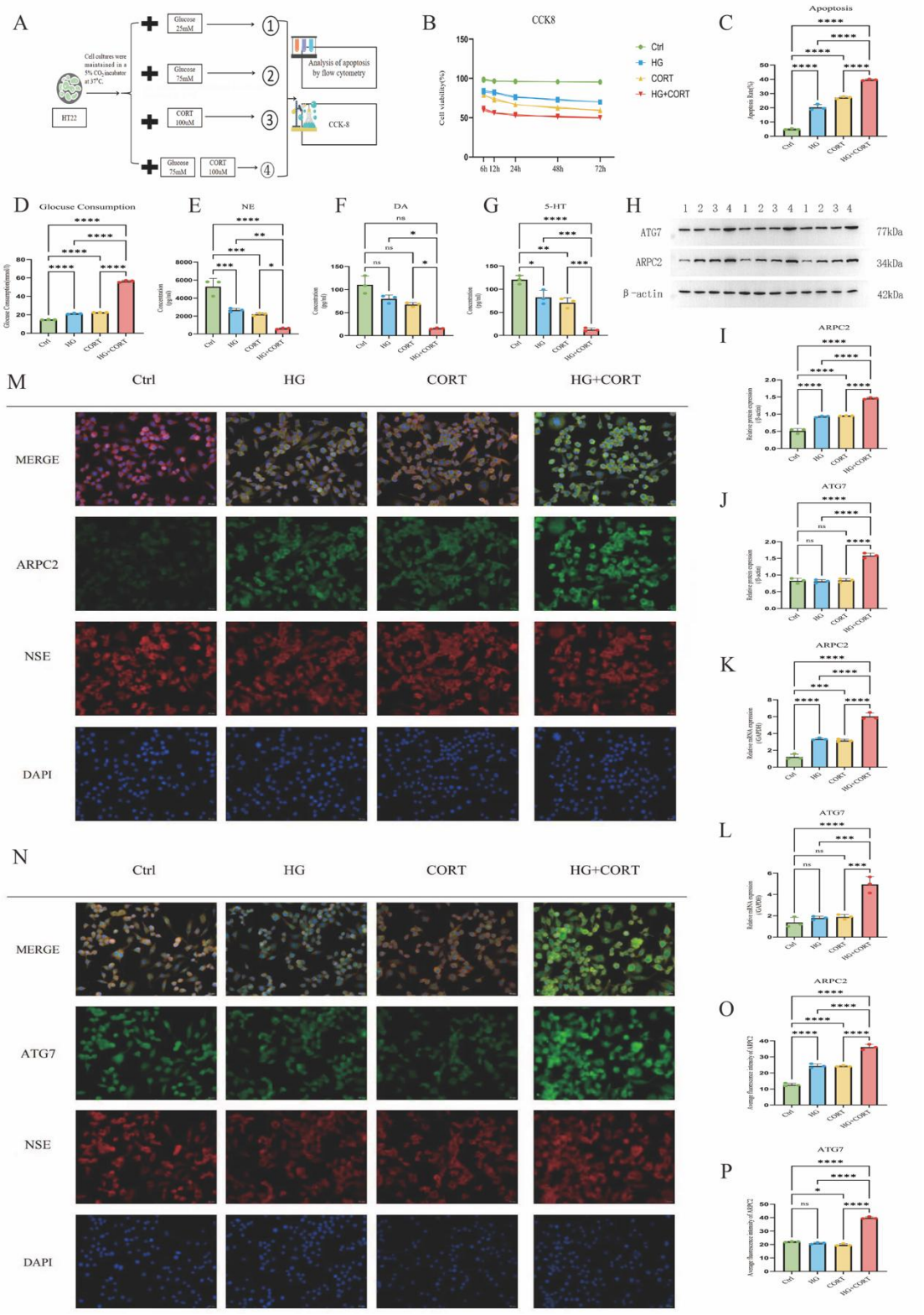


**Figure 6. Cellular validation of ARPC2 and ATG7 upregulation under combined high-glucose and cortisol treatment.**

**(A)** Schematic diagram of the cellular modeling protocol (Ctrl, HG, CORT, and HG + CORT groups).

**(B)** Cell viability assessed by CCK8 assay at different time points.

**(C)** Apoptosis rate in each treatment group.

**(D)** Glucose consumption in each group.

**(E-G)** Neurotransmitters levels in culture supernatants, including norepinephrine (NE) (E), dopamine (DA) (F), and 5-hydroxytryptamine (5-HT) (G).

**(H)** Representative WB images of ARPC2 and ATG7 expression (1 = Ctrl, 2 = HG, 3 = CORT, 4 = HG + CORT).

**(I-J)** Quantification of ARPC2 (I) and ATG7 (J) protein expression.

**(K-L) q**PCR of ARPC2 (K) and ATG7 (L) mRNA expression.

**(M-N) Immunofluorescence staining showing the colocalization of** ARPC2 (M) or ATG7 (N) with neuron-specific enolase (NSE)

**(O-P)** Quantification of ARPC2 (O) and ATG7 (P) immunofluorescence intensity. (ns = not significant, *$P < 0.05$, **$P < 0.01$, ***$P < 0.001$, ****$P < 0.0001$).

ARPC2 and ATG7 expression was assessed in DM and DD to evaluate molecular alterations and mechanisms. ARPC2 protein expression was significantly upregulated in both the HG and CORT group compared with the Ctrl group (Figure 6H–J) ($P < 0.0001$) and was further upregulated in the HG + CORT group compared with the HG and CORT groups ($P < 0.0001$). ARPC2 and ATG7 mRNA expression was significantly higher in the HG + CORT group than in the HG and CORT groups (Figure 6K-L) ($P < 0.001$).

Immunofluorescence double staining demonstrated colocalization of ARPC2 and ATG7 with the neuronal marker neuron-specific enolase (NSE). NSE showed prominent cytoplasmic localization in neurons, and ARPC2 and ATG7 showed clear cytoplasmic localization. Merged images revealed substantial overlap of fluorescence signals within the cytoplasm, confirming neuronal expression. Moreover, ARPC2 and ATG7 expression were higher in the HG + CORT group than in the HG and CORT groups (Figure 6M-P) ($P < 0.0001$).

4. Discussion

DD and DM represent two major global health challenges characterized by high comorbidity rates. In this study, the immune system was considered the central focus, leveraging large-scale genetic and expression datasets, with IRGs used as the starting point. The potential roles of ARPC2 and ATG7 in the comorbidity mechanisms of DM and DD were explored. Functional enrichment analysis confirmed their involvement in key pathways, including autophagy and immune response. Immune infiltration analysis further highlighted their association with immune cell dysregulation. Subsequent *in vitro* and *in vivo* experiments demonstrated that both genes were upregulated in the DM-DD state, suggesting their potential participation in the pathogenesis and progression of comorbidity.

ARPC2 is an actin-binding component involved in the regulation of actin polymerization, mediating the formation of branched actin networks, and interacting with parent actin filaments (Cheng et al., 2019). ARPC2 is widely expressed across multiple tissues and cell types (Huang et al., 2022). As a subunit of the Arp2/3 complex, it participates in cytoskeletal remodeling, cell motility, endocytosis, and immune cell activation (Daugherty and Goode, 2008). It is also involved in biological processes, including immune activation, phagocytosis, and tumor migration (Liu et al., 2024) and is associated with disease development, including tumor progression, ulcerative colitis, and dry eye syndrome (Cheng et al., 2019; Franke et al., 2008; Liu et al., 2024). Elevated ARPC2 expression in CD4+ T cells is associated with increased risk of Parkinson's disease (Wu et al., 2025), suggesting a potential role in neuroinflammation. Additionally, ARPC2 is a key hub gene in subthreshold symptomatic depression (Hu et al., 2021). ARPC2 also participates in cytoskeletal remodeling during FcγR-mediated phagocytosis and is involved in autophagy-related immune activation, potentially exacerbating inflammatory responses and tissue damage (Liu et al., 2024). ARPC2 exacerbates neuroinflammation, neuronal apoptosis and chronic inflammatory responses, thereby contributing to cognitive decline (Picca et al., 2020). In the present study, *in vitro* and *in vivo* experiments demonstrated elevated ARPC2 expression in DM, DD, and DM-DD mice and cells, consistent with

previously reported abnormal ARPC2 expression in type 2 DM mice (Edhager et al., 2018).

ATG7 belongs to the ATG family and promotes autophagosome formation through ubiquitin-like conjugation systems involving LC3. Its primary function is to mediate the ubiquitination-like activation of autophagy-related proteins, thereby initiating autophagosome formation. Recent studies demonstrated that ATG7 is involved not only in canonical autophagy but in non-autophagy-dependent biological processes, including immunomodulation, cell death, protein secretion, and cell cycle regulation. ATG7 dysfunction is associated with autophagy impairment and protein aggregation in diseases such as Alzheimer's disease, Parkinson's disease, and amyotrophic lateral sclerosis, where it may function as a disease progression promoter rather than a primary causative factor (Collier et al., 2021b). In intestinal inflammation models, ATG7 regulates Th1/Treg differentiation through the modulation of Ets1 expression, thereby alleviating mucosal inflammation. ATG7 also sustains the autophagy flux, facilitating the clearance of abnormal proteins and organelles, and protecting neurons from toxic accumulation and functional impairment (Collier et al., 2021a). In these diseases, ATG7 exerts a protective role in disease progression, whereas its role in comorbidities is opposite. The autophagy pathway involving ATG7 acts in depression and diabetes pathogenesis (Lim et al., 2014; Sun et al., 2024). Under high-glucose conditions, excessive ATG7 expression promotes autophagy overactivation and induces apoptosis in endothelial progenitor cells, thus impairing vascular repair (Tian et al., 2020). Similarly, increased ATG7 expression in endothelial cells under high-fat diet conditions leads to weight gain, insulin resistance, fatty liver, and inflammation in adipose tissue (Ren et al., 2025). Under comorbidity conditions, ATG7 may exacerbate disease progression through the dysregulated autophagy activation. A promoting role of ATG7 in depression has also been reported, as BRD2 LLPS-mediated activation of the ATG7 super-enhancer has been linked to depressive pathology (Li et al., 2025). In contrast, Henriksen et al. reported reduced ATG7 expression in DM patients (Henriksen et al., 2019). This discrepancy may reflect differences in tissue specificity, disease stage, and metabolic context. In the present

study, transcriptomic analyses were based on blood-derived datasets, whereas experimental validation was performed in hippocampal and pancreatic tissues, as well as in a combined high-glucose and cortisol neuronal model. ATG7 expression is known to be dynamically regulated across tissues with distinct metabolic demands and may shift during different phases of disease progression (Lim et al., 2014; Sun et al., 2024). Under high-glucose or high-fat conditions, excessive ATG7 expression has been associated with autophagy overactivation and metabolic dysfunction (Tian et al., 2020; Ren et al., 2025). Therefore, in early or isolated DM, autophagy impairment may be associated with reduced ATG7 expression (Henriksen et al., 2019), whereas under combined metabolic and neuroendocrine stress conditions, such as those modeled in the present DM-DD context, compensatory or pathological upregulation of ATG7 may occur. The increased ATG7 expression observed in the DM-DD state may thus represent a context-dependent response to sustained metabolic and inflammatory stress rather than a direct contradiction of previous findings (Lim et al., 2014; Sun et al., 2024). Similarly, the autophagy pathway involving ATG7 has been confirmed by multiple studies as associated with the pathogenesis of depression and diabetes (Lim et al., 2014; Sun et al., 2024).

Although ARPC2 and ATG7 differ in structure and function, both are involved in immune regulation and autophagy-related processes. In this study, GO and KEGG enrichment analysis revealed enrichment of immune and autophagy-related pathways and positive correlations with immune cell dysregulation were observed, suggesting that these genes may influence comorbidity through the regulation of neuroinflammation, autophagy, and immune imbalance. NSE-based immunofluorescence and subcellular localization analyses were performed to further clarify their cellular distribution. ARPC2 was distributed in the cytoplasm and nucleus of HT22 cells, and its expression increased under HG, CORT, and particularly HG + CORT conditions. This suggests that ARPC2 may function as a stress-responsive molecule linking metabolic and hormonal stressors to immune dysregulation. Its nuclear localization suggested potential regulatory roles beyond cytoskeletal organization. Further research is required to clarify the underlying mechanisms by

which the disease progresses. ATG7 exhibited dynamic and context-dependent expression patterns and was localized in both cytoplasm and nucleus. ATG7 expression was downregulated under CORT treatment alone compared with the Ctrl group, but was restored and elevated in the presence of HG. This pattern suggested that ATG7 may function as an integrative node at the intersection of metabolic and neuroendocrine stress pathways. This synergistic upregulation observed under HG + CORT conditions may reflect a compensatory or pathological feedback involving autophagic flux and inflammatory signaling, which warrants further investigation. Drug prediction and molecular docking were also performed to identify potential therapeutic interactions. The highest predicted binding affinity was observed between ARPC2 and the drug Menogaril, while ATG7 showed the strongest affinity with Pentylenetertrazole. Although these results do not represent clinical evidence, they further support the potential of ARPC2 and ATG7 as therapeutic targets.

This study innovatively applied MR analysis to strengthen the genetic evidence supporting causal associations between specific genes and disease risk, reducing potential confounding inherent in observational studies. A significant strength lies in the translational validation strategy, whereby transcriptomics and MR-based predictions were substantiated through *in vitro* and *in vivo* expression analysis. However, several limitations should be acknowledged. Although differential expression was confirmed in cellular and animal models, functional genetic manipulation (e.g., knockdown or overexpression) was not performed to delineate downstream mechanisms. Furthermore, validation in independent clinical cohorts is required to determine whether ARPC2 and ATG7 expression is consistently associated with DM-DD comorbidity in human populations.

## 5. Conclusion

ARPC2 and ATG7 were identified as candidate immune-related biomarkers associated with the comorbidity of DM and DD. Under comorbid conditions, upregulation of these two genes may contribute to disease progression through the modulation of immune activation and autophagy-related pathways. These findings

provide additional insights into the shared immune-mediated mechanisms underlying DM and DD, and highlight ARPC2 and ATG7 as potential targets for future diagnostic and therapeutic explorations.

**Abbreviations**

AD Alzheimer's disease

ARPC2 Actin-related protein 2/3 complex subunit 2

ATG7 Autophagy-related protein 7

CC Cellular component

CON/Ctrl Control

BP Biological process

DCA Decision curve analysis

DM Diabetes mellitus

DD Depressive disorder

FBS fetal bovine serum

GO Gene Ontology

IRGs Immune-related genes

KEGG Kyoto Encyclopedia of Genes and Genomes

MF Molecular function

MR Mendelian randomization

PD Parkinson's disease

q-PCR Quantitative polymerase chain reaction

STZ Streptozotocin

**6.CRediT authorship contribution statement**

**Li Shi、Dandan Huang、Linkuai Zhu**:Writing – review & editing, Writing – original draft, Visualization, Methodology, Investigation, Conceptualization, Data curation, Formal analysis.**Li Zhu、Na Li、Yang Liu**: Methodology. **Yan Jiang、YuShan Xu**:Writing – review & editing, Supervision, Funding acquisition, Conceptualization.

**7. Founding**

This work was supported by The Science and Technology Program Project of the Yunnan Provincial Department of Science and Technology (Grant No.

202301AY070001-290 to Li Shi)；Yunnan Clinical Medical Center for Endocrine and Metabolic Diseases Research Project(Grant Nos. 2024YNLCYXZX0074 to Li Shi; 2024YNLCYXZX0069 to Yan Jiang;2024YNLCYXZX0076 to Yushan Xu);The Funding of the Young Talents Project of the Support Plan for the Talents of Xing dian (Grant No. RLQ820220008 to Li Shi);Yunnan Clinical Medical Center for Endocrine and Metabolic Diseases（Grant No. 202505AJ310007 to Yushan Xu）；Major Research Project on Cancer, Cardiovascular, Respiratory, and Metabolic Diseases Prevention and Treatment under the Science and Technology Innovation 2030 Initiative（Grant No.2023ZD0509200 to Yan Jiang).

## 8. Declaration of competing interest

The authors have no potential conflicts of interest to declare.

## 9. Ethical Statement:

The study data were sourced from the public database GEO. The original database has obtained the necessary ethical approvals and patient informed consent, and no additional review by the institutional ethics committee is required.

## 10.References

Cheng, Z., Wei, W., Wu, Z., Wang, J., Ding, X., Sheng, Y., Han, Y., Wu, Q., 2019. ARPC2 promotes breast cancer proliferation and metastasis. Oncol. Rep. 41, 3189–3200. https://doi.org/10.3892/or.2019.7113

Collier, J.J., Oláhová, M., McWilliams, T.G., Taylor, R.W., 2021a. ATG7 safeguards human neural integrity. Autophagy 17, 2651–2653. https://doi.org/10.1080/15548627.2021.1953267

Collier, J.J., Suomi, F., Oláhová, M., McWilliams, T.G., Taylor, R.W., 2021b. Emerging roles of ATG7 in human health and disease. EMBO Mol. Med. 13, e14824. https://doi.org/10.15252/emmm.202114824

Daugherty, K.M., Goode, B.L., 2008. Functional surfaces on the p35/ARPC2 subunit of Arp2/3 complex required for cell growth, actin nucleation, and endocytosis. J. Biol. Chem. 283, 16950–16959. https://doi.org/10.1074/jbc.M800783200

Duarte-Silva, E., de Melo, M.G., Maes, M., Filho, A.J.M.C., Macedo, D., Peixoto, C.A., 2021. Shared metabolic and neuroimmune mechanisms underlying Type 2 Diabetes Mellitus and Major Depressive Disorder. Prog. Neuropsychopharmacol. Biol. Psychiatry 111, 110351. https://doi.org/10.1016/j.pnpbp.2021.110351

Edhager, A.V., Povlsen, J.A., Løfgren, B., Bøtker, H.E., Palmfeldt, J., 2018. Proteomics of the Rat Myocardium during Development of Type 2 Diabetes Mellitus Reveals Progressive Alterations in Major Metabolic Pathways. J.

Proteome Res. 17, 2521–2532. https://doi.org/10.1021/acs.jproteome.8b00276

Franke, A., Balschun, T., Karlsen, T.H., Sventoraityte, J., Nikolaus, S., Mayr, G., Domingues, F.S., Albrecht, M., Nothnagel, M., Ellinghaus, D., Sina, C., Onnie, C.M., Weersma, R.K., Stokkers, P.C.F., Wijmenga, C., Gazouli, M., Strachan, D., McArdle, W.L., Vermeire, S., Rutgeerts, P., Rosenstiel, P., Krawczak, M., Vatn, M.H., IBSEN study group, Mathew, C.G., Schreiber, S., 2008. Sequence variants in IL10, ARPC2 and multiple other loci contribute to ulcerative colitis susceptibility. Nat. Genet. 40, 1319–1323. https://doi.org/10.1038/ng.221

Gillett, A.C., Hagenaars, S.P., Handley, D., Casanova, F., Young, K.G., Green, H., Lewis, C.M., Tyrrell, J., 2024. The impact of major depressive disorder on glycaemic control in type 2 diabetes: a longitudinal cohort study using UK Biobank primary care records. BMC Med. 22, 211. https://doi.org/10.1186/s12916-024-03425-9

Habib, S., Sangaraju, S.L., Yepez, D., Grandes, X.A., Talanki Manjunatha, R., 2022. The Nexus Between Diabetes and Depression: A Narrative Review. Cureus 14, e25611. https://doi.org/10.7759/cureus.25611

He, R., Guan, C., Zhao, X., Yu, L., Cui, Y., 2024. Expression of immune related genes and possible regulatory mechanisms in different stages of non-alcoholic fatty liver disease. Front. Immunol. 15, 1364442. https://doi.org/10.3389/fimmu.2024.1364442

Henriksen, T.I., Wigge, L.V., Nielsen, J., Pedersen, B.K., Sandri, M., Scheele, C., 2019. Dysregulated autophagy in muscle precursor cells from humans with type 2 diabetes. Sci. Rep. 9, 8169. https://doi.org/10.1038/s41598-019-44535-2

Ho-Plágaro, A., Rodríguez-Díaz, C., Santiago-Fernández, C., López-Gómez, C., García-Serrano, S., Martín-Reyes, F., Rodríguez-Pacheco, F., Rodríguez-Cañete, A., Alcaín-Martínez, G., Vázquez-Pedreño, L., Valdés, S., Garrido-Sánchez, L., García-Fuentes, E., 2022. Morbid Obesity in Women Is Associated with an Altered Intestinal Expression of Genes Related to Cancer Risk and Immune, Defensive, and Antimicrobial Response. Biomedicines 10, 1024. https://doi.org/10.3390/biomedicines10051024

Hu, G., Yu, S., Yuan, C., Hong, W., Wang, Z., Zhang, R., Wang, D., Li, Z., Yi, Z., Fang, Y., 2021. Gene expression signatures differentiating major depressive disorder from subsyndromal symptomatic depression. Aging 13, 13124–13137. https://doi.org/10.18632/aging.202995

Huang, S., Dong, C., Li, D., Xu, Y., Wu, J., 2022. ARPC2: A Pan-Cancer Prognostic and Immunological Biomarker That Promotes Hepatocellular Carcinoma Cell Proliferation and Invasion. Front. Cell Dev. Biol. 10, 896080. https://doi.org/10.3389/fcell.2022.896080

Khawagi, W.Y., Al-Kuraishy, H.M., Hussein, N.R., Al-Gareeb, A.I., Atef, E., Elhussieny, O., Alexiou, A., Papadakis, M., Jabir, M.S., Alshehri, A.A., Saad, H.M., Batiha, G.E.-S., 2024. Depression and type 2 diabetes: A causal relationship and mechanistic pathway. Diabetes Obes. Metab. 26, 3031–3044. https://doi.org/10.1111/dom.15630

Li, S., Yang, D., Zhou, X., Chen, L., Liu, L., Lin, R., Li, X., Liu, Y., Qiu, H., Cao, H., Liu, J., Cheng, Q., 2024. Neurological and metabolic related pathophysiologies and treatment of comorbid diabetes with depression. CNS Neurosci. Ther. 30, e14497. https://doi.org/10.1111/cns.14497

Li, Z., Wang, X., Li, Q., Liu, Y., Si, W., Chen, D., Wang, Q., Zhu, M., 2025. BRD2 phase separation activates super-enhancer-driven ATG7 transcription to promote ferritinophagy in depression. Sci. Rep. 15, 37493. https://doi.org/10.1038/s41598-025-21631-0

Lim, Y.-M., Lim, H., Hur, K.Y., Quan, W., Lee, H.-Y., Cheon, H., Ryu, D., Koo, S.-H., Kim, H.L., Kim, J., Komatsu, M., Lee, M.-S., 2014. Systemic autophagy insufficiency compromises adaptation to metabolic stress and facilitates progression from obesity to diabetes. Nat. Commun. 5, 4934. https://doi.org/10.1038/ncomms5934

Liu, P., Jiang, P., Yu, Y., Tan, K., Qin, G.-Y., Liu, T., Tian, S., Peng, J., Peng, Q., 2024. Modified Danzhi Xiaoyao Powder (MDXP) improves the corneal damage in dry eye disease (DED) mice through phagocytosis. J. Ethnopharmacol. 321, 117544. https://doi.org/10.1016/j.jep.2023.117544

Lu, X., Xie, Q., Pan, X., Zhang, R., Zhang, X., Peng, G., Zhang, Y., Shen, S., Tong, N., 2024. Type 2 diabetes mellitus in adults: pathogenesis, prevention and therapy. Signal Transduct. Target. Ther. 9, 262. https://doi.org/10.1038/s41392-024-01951-9

Maina, J.G., Balkhiyarova, Z., Nouwen, A., Pupko, I., Ulrich, A., Boissel, M., Bonnefond, A., Froguel, P., Khamis, A., Prokopenko, I., Kaakinen, M., 2023. Bidirectional Mendelian Randomization and Multiphenotype GWAS Show Causality and Shared Pathophysiology Between Depression and Type 2 Diabetes. Diabetes Care 46, 1707–1714. https://doi.org/10.2337/dc22-2373

Picca, A., Calvani, R., Coelho-Junior, H.J., Landi, F., Bernabei, R., Marzetti, E., 2020. Mitochondrial Dysfunction, Oxidative Stress, and Neuroinflammation: Intertwined Roads to Neurodegeneration. Antioxid. Basel Switz. 9, 647. https://doi.org/10.3390/antiox9080647

Ren, G., Bhatnagar, S., Young, M.E., Lee, T., Kim, J.-A., 2025. Endothelial autophagy-related gene 7 contributes to high fat diet-induced obesity. Mol. Metab. 93, 102099. https://doi.org/10.1016/j.molmet.2025.102099

Sarwar, H., Rafiqi, S.I., Ahmad, S., Jinna, S., Khan, S.A., Karim, T., Qureshi, O., Zahid, Z.A., Elhai, J.D., Levine, J.C., Naqvi, S.J., Jaume, J.C., Imam, S., 2022. Hyperinsulinemia Associated Depression. Clin. Med. Insights Endocrinol. Diabetes 15, 11795514221090244. https://doi.org/10.1177/11795514221090244

Song, J., Ma, Z., Zhang, H., Liang, T., Zhang, J., 2023. Identification of novel biomarkers linking depressive disorder and Alzheimer's disease based on an integrative bioinformatics analysis. BMC Genomic Data 24, 22. https://doi.org/10.1186/s12863-023-01120-x

Sudirman, S., Hwang, Y.-Y., Su, C.-H., Lu, T.-Y., Kuo, H.-P., Hwang, D.-F., Kong, Z.-L., 2024. Blue mussel (Mytilus edulis) water extract ameliorates intestinal

immune response in high-fat diet-streptozotocin-induced diabetic mice. Food Funct. 15, 9357–9367. https://doi.org/10.1039/d3fo04639g

Sun, Y., Zhao, Y., Lu, Y., Li, H., Xiang, J., Yang, D., Wang, J., Gao, X., Wang, Y., 2024. Urinary stem cell-derived exocrine circRNA ATG7 regulates the SOCS1/STAT3 signaling pathway through miR-4500, inhibits M1 macrophage polarization, and alleviates the progression of diabetes nephropathy. Int. Urol. Nephrol. 56, 1449–1463. https://doi.org/10.1007/s11255-023-03819-3

Tian, D., Xiang, Y., Tang, Y., Ge, Z., Li, Q., Zhang, Y., 2020. Circ-ADAM9 targeting PTEN and ATG7 promotes autophagy and apoptosis of diabetic endothelial progenitor cells by sponging mir-20a-5p. Cell Death Dis. 11, 526. https://doi.org/10.1038/s41419-020-02745-x

Wilson, J.B., Epstein, M., Lopez, B., Brown, A.K., Lutfy, K., Friedman, T.C., 2023. The role of Neurochemicals, Stress Hormones and Immune System in the Positive Feedback Loops between Diabetes, Obesity and Depression. Front. Endocrinol. 14, 1224612. https://doi.org/10.3389/fendo.2023.1224612

Wimberley, T., Horsdal, H.T., Brikell, I., Laursen, T.M., Astrup, A., Fanelli, G., Bralten, J., Poelmans, G., Gils, V.V., Jansen, W.J., Vos, S.J.B., Bertaina-Anglade, V., Camacho-Barcia, L., Mora-Maltas, B., Fernandez-Aranda, F., Bonet, M.B., Salas-Salvadó, J., Franke, B., Dalsgaard, S., 2022. Temporally ordered associations between type 2 diabetes and brain disorders – a Danish register-based cohort study. BMC Psychiatry 22, 573. https://doi.org/10.1186/s12888-022-04163-z

Wu, X., Wang, K., Li, Q., Zhang, Y., Wei, P., Shan, Y., Zhao, G., 2025. Combining Single-Cell RNA Sequencing and Mendelian Randomization to Explore Novel Drug Targets for Parkinson's Disease. Mol. Neurobiol. 62, 7380–7392. https://doi.org/10.1007/s12035-025-04700-3

Yadav, S., Hong, Y.-R., Westen, S., Marlow, N.M., Haller, M.J., Walker, A.F., 2023. Sociodemographic factors associated with major depressive episodes and suicidal ideation among emerging adults with diabetes in the U.S. Front. Endocrinol. 14, 1276336. https://doi.org/10.3389/fendo.2023.1276336

Yao, J., Zhu, C.-Q., Sun, Y., Huang, Y.-W., Li, Q.-H., Liao, H.-M., Deng, X.-J., Li, W.-M., 2025. Insulin resistance: The role in comorbid type 2 diabetes mellitus and depression. Neurosci. Biobehav. Rev. 175, 106218. https://doi.org/10.1016/j.neubiorev.2025.106218

Yu, M.G., Gordin, D., Fu, J., Park, K., Li, Q., King, G.L., 2024. Protective Factors and the Pathogenesis of Complications in Diabetes. Endocr. Rev. 45, 227–252. https://doi.org/10.1210/endrev/bnad030

Zhang, X., Wang, P., Shi, L., Li, N., 2021. Study on caspase-1 and partial cognitive impairment in the comorbidity of type 2 diabetes and MDD. J. Affect. Disord. 290, 387–392. https://doi.org/10.1016/j.jad.2021.04.092

Zhou, D., Zhou, T., Tang, S., Li, Q., Li, W., Gan, G., Li, M., Chen, Q., 2024. Network pharmacology combined with Mendelian randomization analysis to identify the key targets of renin-angiotensin-aldosterone system inhibitors in the treatment of diabetic nephropathy. Front. Endocrinol. 15, 1354950.

https://doi.org/10.3389/fendo.2024.1354950
Zhou, Z., Wang, H., Tan, S., Zhang, H., Zhu, Y., 2024. The alterations of innate immunity and enhanced severity of infections in diabetes mellitus. Immunology 171, 313–323. https://doi.org/10.1111/imm.13706

## Supplementary Files

This is a list of supplementary files associated with this preprint. Click to download.

- SupportinginformationTable.xlsx